# A Dual-Threshold ATI-SAR Approach for Detecting Slow Moving Targets

Yuhong Zhang, Ph. D., Stiefvater Consultants
Abdelhak Hajjari, Ph. D. Research Associates for Defense Conversion Inc.
Kyungjung Kim, Ph. D., Stiefvater Consultants
Braham Himed, Ph. D., Air Force Research Lab/SNRT

Key Words: along-track, interferometry, synthetic aperture radar (SAR), ground moving target indication (GMTI)

*ABSTRACT*

The high false alarm associated with conventional along-track interferometric synthetic aperture radar (ATI-SAR) is a big concern for any valuable military radar. To reduce the false alarm rate, this paper proposes a dual-threshold approach that combines the conventional interferometric phase detection with the SAR image amplitude detection. This yields two results: (1) the interferometric phase map (including target velocity information) obtained by applying the interferometric phase detection only to the pixels selected by the amplitude detection, and (2) the amplitude map (including target strength information) obtained by applying the amplitude detection only to the pixels selected by the interferometric phase detection. The concept is illustrated by the results obtained using the Jet Propulsion Laboratory's (JPL) AirSAR ATI data, collected in the Monterey Bay area, California. The ATI-SAR processing requires also a precise calibration of the platform's crab angle. This paper presents a simple blind-calibration method that does not require any knowledge of the background and/or the actual crab angle.

## 1. *INTRODUCTION*

The ATI-SAR technique has been proven valuable to sense the earth-surface motion such as ocean surface currents. Recently, there has been increasing interest in applying ATI-SAR techniques to detect slow moving target detection, especially ground moving target indication (GMTI) using space-based assets [1].

ATI-SAR is based on the acquisition of two complex SAR images taken under identical geometries separated by a short time interval. The phase difference between the two interferometric images is used as a test statistic to be compared with a decision threshold. The question then is whether ATI-SAR could be used for detecting slow moving targets. In this paper, we propose to examine the detection performance of conventional ATI-SAR. It is shown that the high false alarm rate associated with this technique would be a big concern for any valuable military radar. To reduce the false alarm rate, this paper proposes a dual-threshold approach that combines the conventional interferometric phase detection with the SAR image amplitude detection. Strong pixels could contain moving targets, stationary objects, and other discretes. The amplitude detection suppresses the weak pixels from large smooth surfaces such as road and water surfaces. This yields two important results:

(1) the interferometric phase map (including target velocity information) obtained by applying the interferometric phase detection only to the pixels selected by the amplitude detection

(2) the amplitude map (including target strength information) obtained by applying the amplitude detection only to the pixels selected by the interferometric phase detection.

The concept is illustrated by the results obtained using JPL's AirSAR ATI data [2], collected in the Monterey Bay, CA area. The ATI-SAR processing requires also a precise calibration of the platform's crab angle. Reference [2] uses a known stationary corner reflector (strong scatterer) array as the reference for the calibration. This paper presents a blind calibration method that does not require any knowledge of the ground reference scatterer and/or the actual crab angle.

## 2. *DETECTION PERFORMANCE OF CONVENTIONAL ATI-SAR*

The ATI-SAR method is based on the acquisition of two complex SAR images (A and B), taken under identical geometries separated by a short time interval, with the interferometric phase being used as a test statistic, as shown in Figure 1.

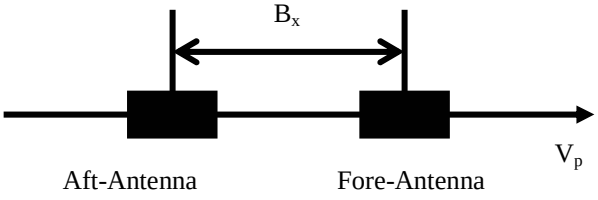


Fore-Antenna, Image A, $t = t_0$
Aft-Antenna, Image B, $t = t_0+\Delta T$, where $\Delta T = B_x / V_p$
The interferometric phase:

$$\theta_v = \frac{4\pi}{\lambda}\frac{B_x}{V_p}V_t$$, where $V_t$ is the target radial speed.

Test Statistic: $\begin{cases} \theta_v \geq \eta_\theta, & H_1 \\ \theta_v < \eta_\theta, & H_0 \end{cases}$

Figure 1. Principles of conventional ATI-SAR.

# Report Documentation Page

*Form Approved*
*OMB No. 0704-0188*



| 1. REPORT DATE | 2. REPORT TYPE | 3. DATES COVERED |
|---|---|---|
| **01 MAY 2005** | **N/A** | **-** |

| 4. TITLE AND SUBTITLE | 5a. CONTRACT NUMBER |
|---|---|
| **A Dual-Threshold ATI-SAR Approach for Detecting Slow Moving Targets** | 5b. GRANT NUMBER |
| | 5c. PROGRAM ELEMENT NUMBER |
| 6. AUTHOR(S) | 5d. PROJECT NUMBER |
| | 5e. TASK NUMBER |
| | 5f. WORK UNIT NUMBER |
| 7. PERFORMING ORGANIZATION NAME(S) AND ADDRESS(ES) **Stiefvater Consultants** | 8. PERFORMING ORGANIZATION REPORT NUMBER |
| 9. SPONSORING/MONITORING AGENCY NAME(S) AND ADDRESS(ES) | 10. SPONSOR/MONITOR'S ACRONYM(S) |
| | 11. SPONSOR/MONITOR'S REPORT NUMBER(S) |

12. DISTRIBUTION/AVAILABILITY STATEMENT
**Approved for public release, distribution unlimited**

13. SUPPLEMENTARY NOTES
**See also ADM002017. Proceedings of the 2005 IEEE International Radar Conference Record Held in Arlington, Virginia on May 9-12, 2005. U.S. Government or Federal Purpose Rights License., The original document contains color images.**

14. ABSTRACT

15. SUBJECT TERMS

| 16. SECURITY CLASSIFICATION OF: | | | 17. LIMITATION OF ABSTRACT | 18. NUMBER OF PAGES | 19a. NAME OF RESPONSIBLE PERSON |
|---|---|---|---|---|---|
| a. REPORT | b. ABSTRACT | c. THIS PAGE | | | |
| **unclassified** | **unclassified** | **unclassified** | **UU** | **5** | |

### 2.1 *False Alarm Rate*

The probability of false alarm (or false alarm rate), $P_{FA}$, can be calculated from the probability density function (pdf) of the interferometric phase in the absence of target. For simplicity, consider a Gaussian clutter associated with a homogeneous background and additive white Gaussian thermal noise. In the absence of target, the interferometric phase is the product of two complex Gaussian correlated signals. The resulting pdf can then be expressed analytically [3] and is strictly dependent on the equivalent correlation coefficient given by

$$\gamma = \frac{\gamma_c}{1 + 1/\mathrm{CNR}} \tag{1}$$

where $\gamma_c$ is the clutter correlation coefficient and CNR is the clutter-to-noise power ratio.

Figure 2 shows the pdf of the interferometric phase in absence of target, for different CNR values and $\gamma_c = 1$ (which represents the best case for ATI-SAR). The corresponding false alarm rates versus (vs.) the phase threshold are shown in Figure 3. The numerical results are listed in Table 1.

Table 1

$P_{FA}$ vs. CNR and phase threshold $\eta_\theta$ (rad.) for $\gamma_c = 1$.

| CNR\ $\eta_\theta$ | 0.5 | 1 | 1.5 | 2 | 2.5 |
|---|---|---|---|---|---|
| 0 dB | 0.66869 | 0.42495 | 0.26718 | 0.16178 | 0.08357 |
| 10 dB | 0.26685 | 0.09902 | 0.04954 | 0.02712 | 0.01339 |
| 20 dB | 0.03996 | 0.01146 | 0.00541 | 0.00291 | 0.00142 |
| 30 dB | 0.00421 | 0.00116 | 0.00054 | 0.00029 | 0.00014 |
| 40 dB | 0.00042 | 0.00011 | 0.00005 | 0.00002 | 0.000014 |

### 2.2 *Probability of Detection*

The pdf in the presence of target is required for computing the probability of detection $P_D$. Unfortunately; this pdf is not analytically available. A Monte Carlo simulation is used in this paper. Figure 4 shows the pdf plots with 100,000 trials for three different values of signal-to-clutter ratio (SCR), for a CNR value of 20dB and $\gamma_c = 1$, and the interferometric phase induced by the target equal to 2 radians. The corresponding $P_D$ plots vs. the phase threshold are shown in Figure 5.

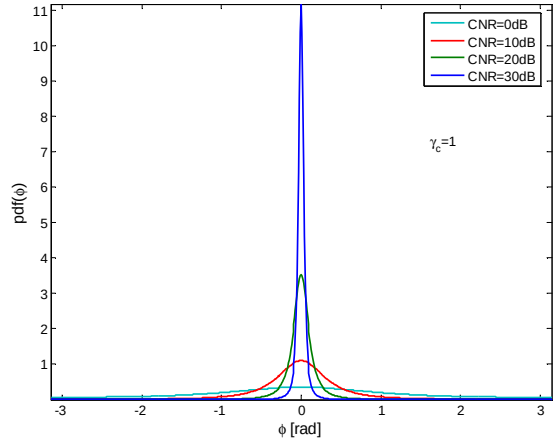


Figure 2. Phase noise *pdf* for different CNR values and $\gamma_c$=1

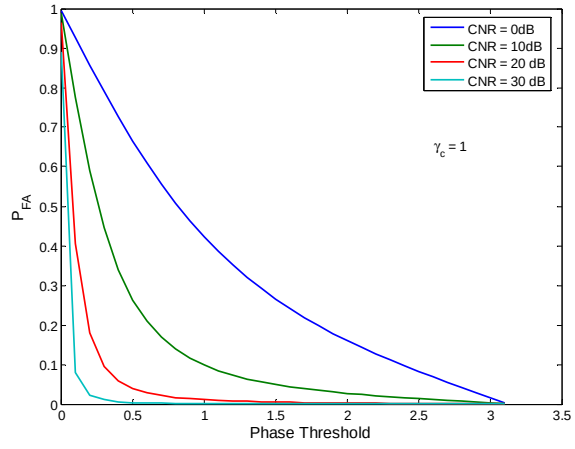


Figure 3. Probability of false alarm for different CNR values and $\gamma_c = 1$

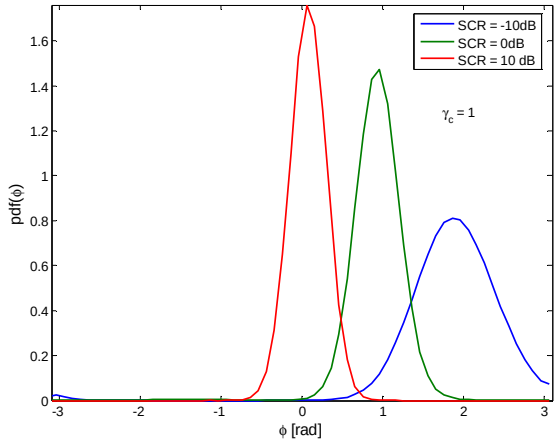


Figure 4. Phase pdf for three different SCR values in presence of a moving target

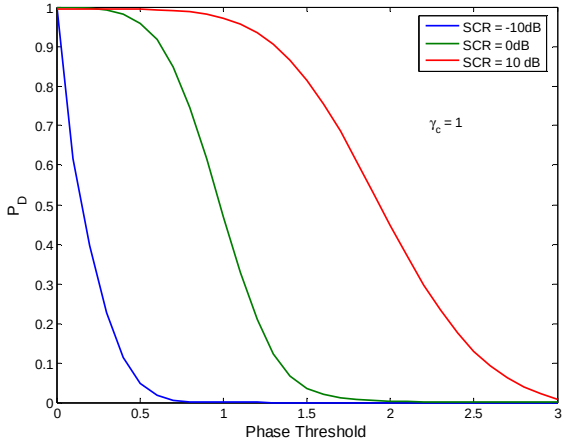


Figure 5. Detection probability for three different SCR values in the presence of a moving target

For example, if $\eta_\theta = 1.5$ radians, then $P_D$ = 0.816 for a 10dB SCR and $P_D$ = 0.036 for a 0dB SCR. From Table 1, we see that the corresponding false alarm rate is $P_{FA} = 5.4 \times 10^{-3}$, which is too high for almost any radar application.

## 3. *DUAL-THRESHOLD DETECTION*

This paper proposes to set another amplitude threshold $\eta_a$ to the SAR amplitude image. Strong pixels could contain moving targets, stationary objects, and other discretes. The amplitude detection suppresses the weak pixels from large smooth surfaces such as road and water surfaces. This detection is similar to the conventional constant false alarm rate (CFAR) processing. There are many algorithms to determine the threshold [4]. The performance depends on the environments. As an example, the threshold is counted relative to the mean amplitude for background in this paper, which is estimated by taking the root mean square (rms) mean value of the median amplitudes (of the corresponding slant-range pixels) over cross-range pixels. For example, setting the amplitude threshold as $\eta_a = 10$ dB means those pixels whose amplitudes are larger than the estimated mean value by 10dB are chosen as candidate target pixels. Jointly using the two thresholds (phase and amplitude), we get two outputs:

(1) The interferometric phase map (target velocity) is obtained by applying the interferometric phase detection only to the pixels selected by the amplitude detection. Specifically, the phase at a pixel will be forced to zero if its image amplitude is below a pre-determined threshold. And,

(2) The amplitude map (target strength) is obtained by applying the amplitude detection only to the pixels selected by the interferometric phase detection.

This concept will be illustrated using JPL's AirSAR ATI data.

## 4. *AIRSAR ATI DATA*

The AirSAR ATI data used in this paper was recorded at L-band in Monterey Bay, California area. The AirSAR system consists of two ATI antennas separated by a distance of 19.7736m.

The strip-map SAR images are obtained using the line-by-line imaging method with N=1024 pulses in a coherent processing interval (CPI), which corresponds to approximately a 3.5m cross-range resolution. Figure 6 shows the SAR image (400 slant range cells for 1.32km, including roads, highways and water) from the data recorded on the Fore-Antenna.

### *4.1 Blind Calibration for Group Phase Shift Induced by Crab Angle*

In the ideal case, two ATI-antennas are aligned with the moving track. However, the crab angle (yaw and pitch) of platform makes two antennas offset from the moving track. Figure 7 illustrates the case where the platform has a yaw angle $\theta_c$, which leads to an offset range in cross-track direction:

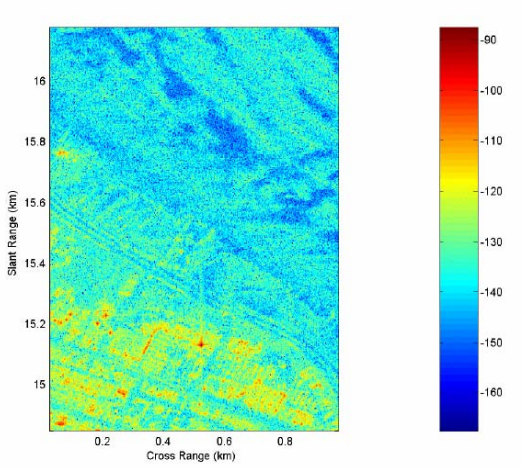


Figure 6. Image A for selected area.

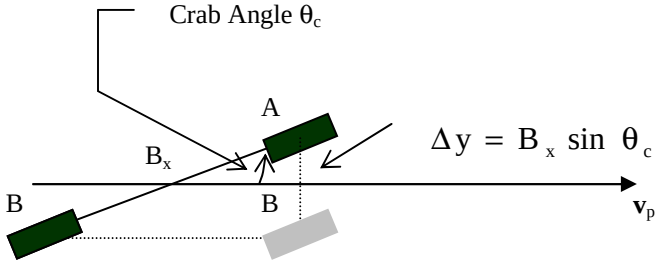


Figure 7. A cross-track offset between two antennas induced by the crab (yaw) angle.

$$\Delta y = B_x \sin \theta_c , \qquad (2)$$

where $B_x$ is the baseline distance. The cross-track offset of two-antennas will induce a phase shift between Images A and B, called group phase shift, which must be calibrated before the ATI-SAR processing. Figure 8 shows the interferometric phase image before the phase calibration. Obviously, phases of most pixels are far from zero.

It is well known that the crab angle varies during the platform motion [2]. Reference [2] uses a known stationary corner reflector (strong scatterer) array on the ground as a reference to calibrate the phase shift. In this paper, we propose a simple blind calibration method that does not require any knowledge of the ground reference scatterers and the actual crab angle. The proposed method first estimates the group phase shift as a function of cross range, and then compensates for this phase shift. Several methods can be used for conducting this estimation procedure. The median phase as a function of cross-range is first calculated and an autoregressive (AR) smoothing processing is then applied to the median phases. The AR-smoothed phase shift is used as an estimate of the true one for calibration purposes. However, it is seen that one estimation and compensation procedure is usually not enough, because the estimation of a group phase shift is based on wrapped interferometric phases

(within $[-\pi, \pi]$), and the compensated phases are wrapped again, which leads to a new group phase shift. An iterative procedure is used in this paper to bypass this problem. It is found that only a few (usually 3 to 5) iterations are needed in most cases. Figure 9 shows the median and AR-smoothed group phase shift as a function of cross-range before phase calibration while Figure 10 shows the corresponding results after calibration. The interferometric phase image after phase compensation is shown in Figure 11. Clearly, the phases of most pixels are now close to zero when compared to Figure 8.

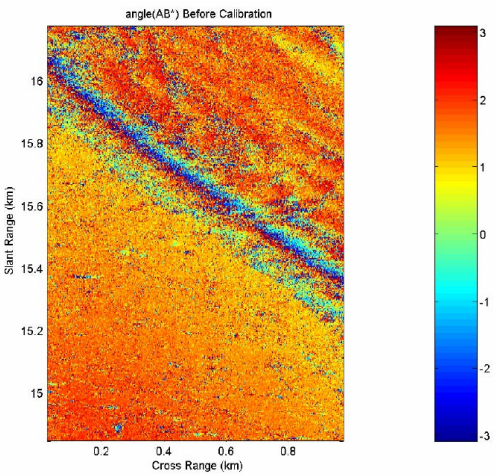


Figure 8. Interferometric phase image before phase calibration

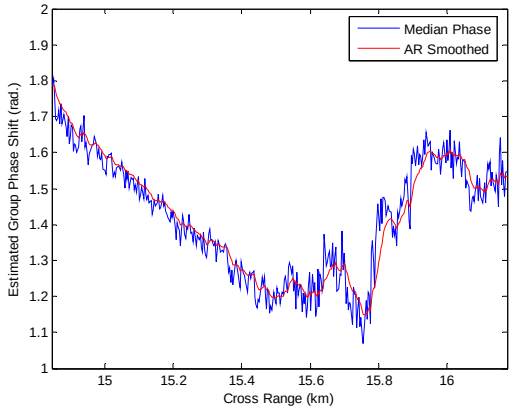


Figure 9. Estimated group phase shift as a function of cross range before phase calibration

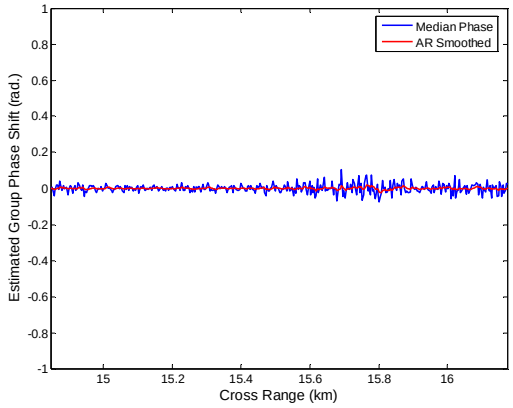


Figure 10. Estimated group phase shift as a function of cross range after phase calibration

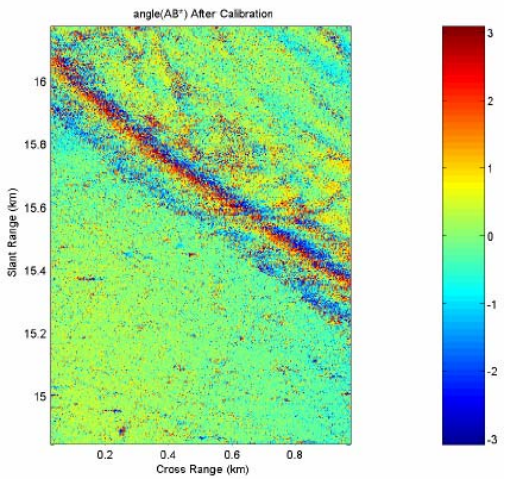


Figure 11. Interferometric phase image after phase calibration

## 5. *RESULTS WITH AIRSAR DATA*

### *5.1 Phase Detection Only*

Phase detection only is the conventional ATI-SAR method. Figure 12 shows the corresponding results with $\eta_\theta = 1.5$ radians. The tidal waves are clearly shown in this image. However, the false alarm rate is too high for surveillance radar applications such as Ground Moving Target Indication (GMTI).

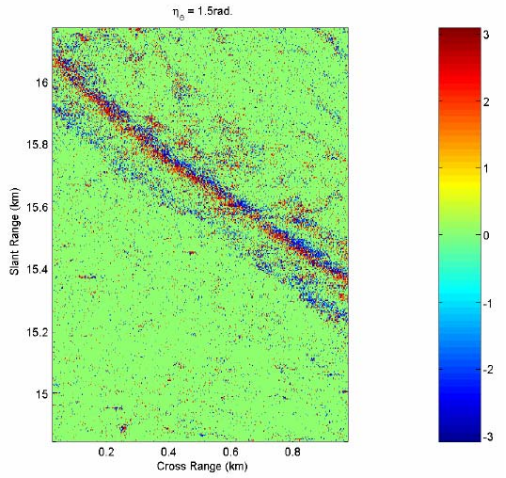


Figure 12. Interferometric phase image with $\eta_\theta = 1.5$ radians

### *5.2 Amplitude Detection Only*

Figure 13 shows the SAR amplitude image trimmed with an amplitude threshold ($\eta_a = 10\text{dB}$) only. This image shows stronger pixels that could possibly contain moving targets, stationary objects, and other discretes. The amplitude-only detection suppresses the weak pixels such as those corresponding to road and water surfaces.

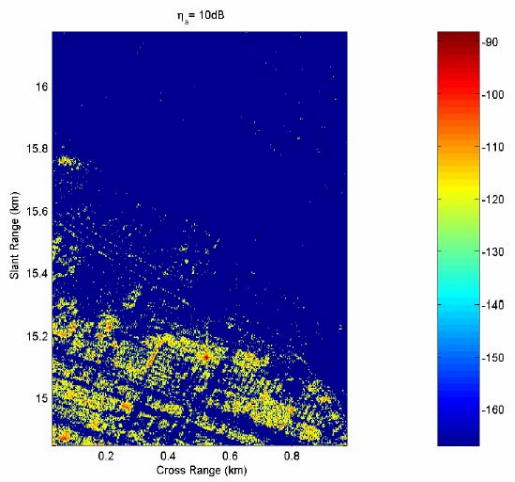


Figure 13. SAR amplitude image with $\eta_a = 10$ dB

### 5.3 *Dual-Threshold Detection*

The dual threshold detection approach proposed in this paper combines the detection results from the above phase and amplitude detection methods. Hence, two important parameters are obtained: phase and amplitude, or velocity and strength. Figure 14 shows the results of the interferometric phase map obtained by applying the amplitude detection results of Figure 13 onto those of Figure 12, i.e., forcing the phase at a pixel to zero if its amplitude is less than the mean value by an amplitude threshold ($\eta_a = 10$ dB here). Clearly, the false alarm rate is dramatically reduced using this approach.

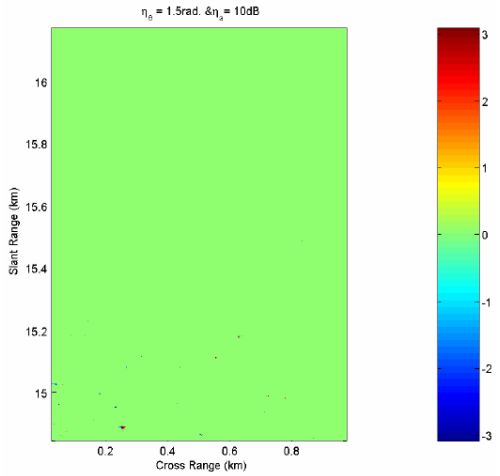


Figure 14. Interferometric phase map with $\eta_\theta = 1.5$ radians and $\eta_a = 10$dB.

Similarly, we can obtain an amplitude map of potential moving targets by applying the phase detection results of Figure 12 onto those of Figure 13, i.e., eliminating the pixels whose phases are below the phase threshold ($\eta_\theta = 1.5$ radians here), as shown in Figure 15, which corresponds to the interferometric phase map of Figure 14. In other words, Figure 14 and Figure 15 show velocity and strength information of possible moving targets. The locations shown in these Figures are shifted from their real ones due to the SAR processing. It is possible to restore the real locations of those slow targets without any interferometric phase ambiguity.

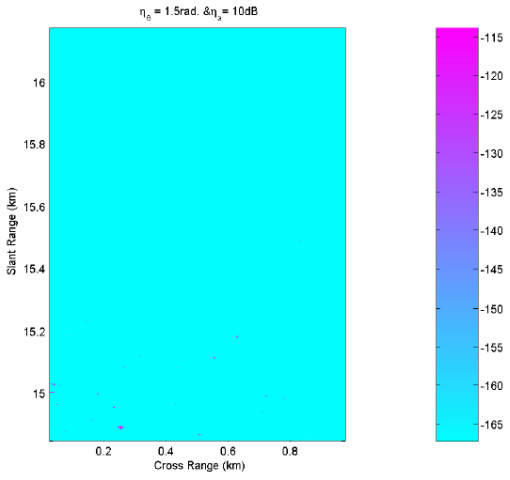


Figure 15. SAR amplitude map with $\eta_\theta = 1.5$ radians and $\eta_a = 10$dB

## 6. *CONCLUSIONS*

Conventional ATI-SAR approaches can detect targets with very low radial speeds, but their false alarm rate is too high if they are to be used in surveillance radars. The proposed dual-threshold approach, which combines the conventional interferometric phase detection and the SAR image amplitude detection, can effectively reduce the false alarm rate. The concept of the dual-threshold approach is illustrated using JPL's AirSAR ATI data. This data is calibrated using a simple blind-calibration procedure. However, this is only a very first try. Future work would include the determination of thresholds and ways to combine them.

## 7. *ACKNOWLEDGEMENT*

The authors would like to thank Dr. Elaine Chapin of JPL for her help in providing and using the AirSAR ATI data.

## 8. *REFERENCES*

1. C. W. Chen, “Performance assessment of along-track interferometry for detecting ground moving targets,” *Proc. 2004 IEEE Radar Conf.*, Philadelphia, PA, April 26-29, 2004.
2. D. A. Imel, "AIRSAR along-track interferometry data," *AIRSAR Earth Science and Applications Workshop*, 4-6 March 2002.
3. R. Bamler and P. Hartl, "Synthetic aperture radar interferometry," *Inverse Problems*, vol. 14, R1-R54, 1998.
4. R. Nitzberg, *Radar Signal Processing and Adaptive Systems*, Artech House, Inc., Norwood, MA, 19999.